Article

Micro Magnetic Field Produced by Fe_3O_4 Nanoparticles in Bone Scaffold for Enhancing Cellular Activity

Shizhen Bin [1,2], Ailun Wang [1], Wang Guo [2] , Li Yu [2] and Pei Feng [2,*]

[1] Research Institute of Light Alloys, Central South University, Changsha 410083, China; shizhenbin@csu.edu.cn (S.B.); walwlz@csu.edu.cn (A.W.)

[2] State Key Laboratory of High Performance Complex Manufacturing, College of Mechanical and Electrical Engineering, Central South University, Changsha 410083, China; guowang@csu.edu.cn (W.G.); yujiali@csu.edu.cn (L.Y.)

[*] Correspondence: fengpei@csu.edu.cn; Tel.: +86-731-88879351; Fax: +86-731-88879044

check for updates

Abstract: The low cellular activity of poly-l-lactic acid (PLLA) limits its application in bone scaffold, although PLLA has advantages in terms of good biocompatibility and easy processing. In this study, superparamagnetic Fe_3O_4 nanoparticles were incorporated into the PLLA bone scaffold prepared by selective laser sintering (SLS) for continuously and steadily enhancing cellular activity. In the scaffold, each Fe_3O_4 nanoparticle was a single magnetic domain without a domain wall, providing a micro-magnetic source to generate a tiny magnetic field, thereby continuously and steadily generating magnetic stimulation to cells. The results showed that the magnetic scaffold exhibited superparamagnetism and its saturation magnetization reached a maximum value of 6.1 emu/g. It promoted the attachment, diffusion, and interaction of MG63 cells, and increased the activity of alkaline phosphatase, thus promoting the cell proliferation and differentiation. Meanwhile, the scaffold with 7% Fe_3O_4 presented increased compressive strength, modulus, and Vickers hardness by 63.4%, 78.9%, and 19.1% compared with the PLLA scaffold, respectively, due to the addition of Fe_3O_4 nanoparticles, which act as a nanoscale reinforcement in the polymer matrix. All these positive results suggested that the PLLA/Fe_3O_4 scaffold with good magnetic properties is of great potential for bone tissue engineering applications.

Keywords: magnetic stimulation; Fe_3O_4 nanoparticles; cellular activity; selective laser sintering; scaffold

1. Introduction

Poly-l-lactic acid (PLLA) has become one of the main bone scaffold materials due to its advantages of good biocompatibility and easy processing [1–3]. Nevertheless, the low cellular activity limits its application in bone tissue engineering due to the lacking of active functional groups and weak cell affinity [4–7]. For enhancing cellular activity, researchers have added various cell growth factors, such as bone morphogenetic protein (BMP), transforming growth factor-beta (TGF-β), fibroblast growth factor, and so on [8–11]. Schofer et al. [8] incorporated BMP-2 into PLLA nanofibers and found that the BMP-2 improved the scaffold's cellular activity by increasing the expression of osteogenic marker proteins and osteogenesis. Zhu et al. [9] added TGF-β1 to nano-HA/PLLA composite scaffold and found that TGF-β1 released and promoted the adhesion, spreading, proliferation of mesenchymal stem cells (MSCs). Although the growth factors can improve cellular activity, they are very expensive and have a decay half-life [12–14]. The fast decay rate makes its biological activity decrease quickly and it cannot be continuously and steadily enhanced, which has greatly limited their wide range of clinical applications.

In recent years, researches have shown that physical stimulation, especially magnetic stimulation, can continuously stimulate cell growth and proliferation, and thus it can be used as an alternative method to increase the cellular activity of bone scaffold [15–17]. Due to its unique magnetic properties, Fe_3O_4 nanoparticles have been receiving considerable interest in biomedical applications [18–20]. When the particle size is less than 30 nm in diameter, the thermal fluctuation energy is equivalent to the magnetocrystalline anisotropy energy, which is enough to cause the whole crystallite to rotate freely, thereby exhibiting superparamagnetism [21,22]. Even if no external magnetic field is applied, the superparamagnetic Fe_3O_4 nanoparticle can be regarded as a single magnetic domain without a domain wall, providing a micro-magnetic source for the nano-scale magnetic field [23,24]. In addition, Fe_3O_4 nanoparticles approved by the Food and Drug Administration (FDA) of United States of America for clinical use, have excellent biocompatibility and safety, and are widely used in bone tissue engineering [25–27]. Taking into account the above characteristics, we suppose that the incorporation of superparamagnetic Fe_3O_4 nanoparticles into the bone scaffold makes it possible for them to generate a large number of tiny magnetic fields in the scaffold, which can activate and enhance cell activity continuously and steadily through magnetic stimulation.

At present, there have been some reports on the research of Fe_3O_4 nanoparticles to enhance cell activity [28–31]. For example, Shan et al. [28] reported that the incorporation of Fe_3O_4 nanoparticles into PLLA fibers enhanced cell adhesion and proliferation without significant cytotoxicity. Wu et al. [29] integrated Fe_3O_4 nanoparticles into CaP bioceramics and found that magnetic fields generated by Fe_3O_4 nanoparticles enhanced the activity of ALP and promoted the differentiation and proliferation of osteoblasts. Wei et al. [30] also indicated that the introduction of magnetic Fe_3O_4 nanoparticles into the CS/PVA fiber membrane could promote cell proliferation and accelerate the bone-like tissue formation. However, all the above studies were basically mainly concentrated on composite materials or fibers, and there were few studies on incorporating Fe_3O_4 nanoparticles into scaffolds for bone regeneration.

In this study, Fe_3O_4 nanoparticles were incorporated into PLLA scaffold via selective laser sintering (SLS) to continuously and stably enhance the cellular activity. The phase composition, thermal properties, magnetic properties, and mechanical properties of the PLLA/Fe_3O_4 scaffolds were comprehensively studied. The effects of the magnetic composite scaffolds on the adhesion, proliferation, and differentiation of MG63 cells are studied, discussed, and explained.

2. Materials and Methods

2.1. Materials

PLLA powders (average particle size: 0.2–5 μm) were purchased from Jinan Daigang Biomaterial Co., Ltd. (Jinan, China). Fe_3O_4 nanoparticles (average particle size: 20 nm) were kindly provided by Shanghai Jichun Industrial Co., Ltd. (Shanghai, China). Dulbecco's Modified Eagle Medium (DMEM), phosphate buffer solution (PBS) and fetus bovine serum (FBS) were purchased from Biological Industries (Beit HaEmek, Israel). MG63 cells were provided by American Type Culture Collection (Manassas, VA, USA). CCK-8 solution was bought from Selleck Chemicals (Houston, TX, USA). All other reagents were purchased from Shanghai Macklin Biochemical Technology Co., Ltd. (Shanghai, China).

2.2. Scaffold Preparation

The preparation process of PLLA/Fe_3O_4 magnetic composite scaffolds included the preparation of composite powders and scaffolds, as schematically depicted in Figure 1. First, the PLLA and Fe_3O_4 powders were weighed in a certain weight ratio (Fe_3O_4 content in the composite: 0, 1, 3, 5, 7, and 9 wt %). Then, the two powders were added into a beaker containing 50 mL of absolute ethanol, and then the mixed solution was ultrasonically dispersed for 30 min. After that, the mixed solution was poured into a ball mill for 1 h for further dispersing. Finally, PLLA/Fe_3O_4 composite powders were

obtained by filtering the mixed solution slowly using a filter paper with pore size of 0.45 µm (Millipore, HAWP01300) and drying in a drying box for 24 h at 50 °C.
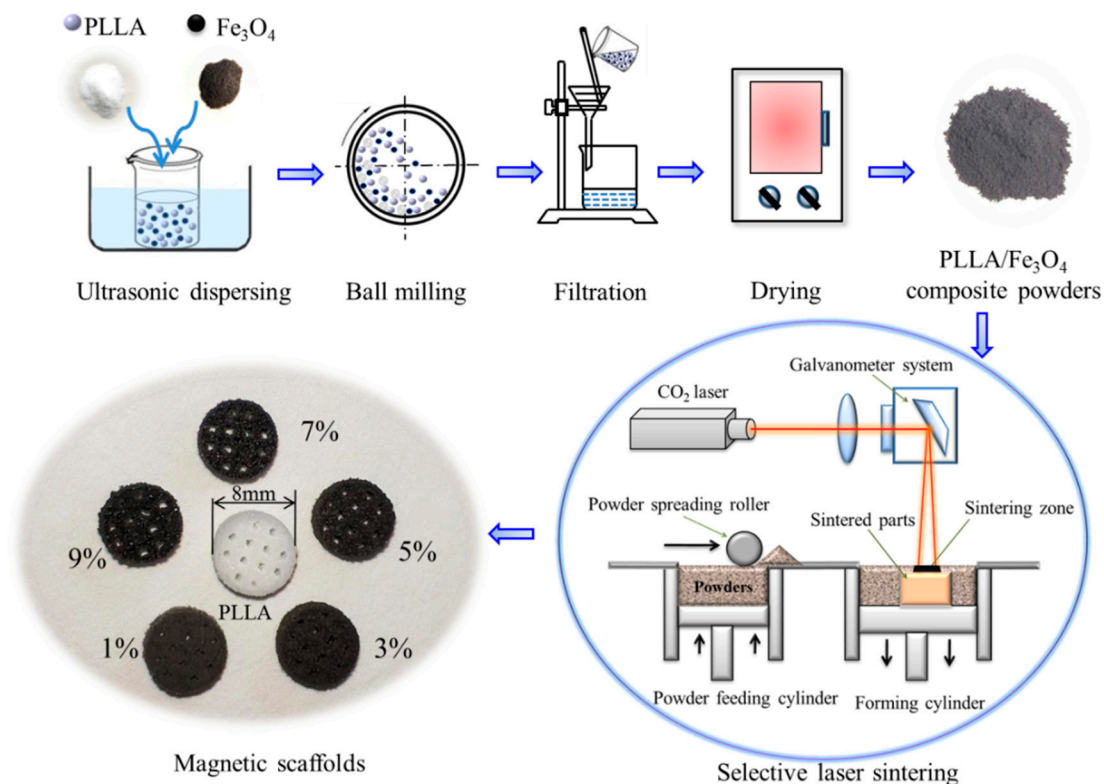
Figure 1. A schematic of the preparation of PLLA/Fe$_3$O$_4$ magnetic composite scaffolds.

The magnetic composite scaffold was prepared by a SLS system with a 100 W CO$_2$ laser ($\lambda = 10.6$ µm) and a galvanometric scanning system. In detail, the powder feeding cylinder piston rises, and then the powder spreading roller evenly lays a layer of powder on the sintering platform. Then under the control of the galvanometric scanning system, the powder layer was scanned and sintered by a laser beam followed the cross-sectional profiles of the model [32]. After sintering a layer, the piston of the forming cylinder was lowered by one layer thickness. Then, the powder spreading roller was controlled to lay a new layer of powder above the previously sintered layer, followed by the next sintering of the powder. The above operation was repeated in this way, and the sintered layers were stacked layer by layer until the whole scaffold was formed. The main process parameters were optimized as follows: scanning speed of 180 mm s^{-1}, scanning interval of 0.15 mm, and layer thickness of 0.1 mm. Six kinds of PLLA/Fe$_3$O$_4$ scaffolds with different contents of Fe$_3$O$_4$ (0, 1, 3, 5, 7, and 9 wt %) were fabricated by SLS, as shown in Figure 1. The optical color of the scaffolds gradually deepens with the increase of Fe$_3$O$_4$ content.

2.3. Characterization

The phase constituent of Fe$_3$O$_4$ nanoparticles and magnetic scaffolds was investigated via XRD (DMAX 2500, Japan Science Co., Tokyo, Japan) at a scan rate of 8°/min in the range of diffraction angle $2\theta = 10°\sim80°$. The chemical group analysis was performed by FTIR (Nicolet 6700, Thermo Electron Scientific Instruments Co., Madison, WI, USA) with a test wavelength of 500 to 4000 cm^{-1} and a number of scans of 16 times. The TGA and DSC curves of the magnetic scaffolds at 30 to 600 °C were measured to evaluate the thermal stability, using a thermo gravimetric analyzer (TGA-105, Nanjing Dazhan Electromechanical Technology Research Institute, Nanjing, China) under nitrogen at a temperature rise rate of 20 °C/min. Magnetic properties of the magnetic composite scaffolds were detected by a vibrating sample magnetometer (VSM7407, Lake Shore Cryotronics Inc., Westerville, OH, USA)

and a permanent magnet. The hysteresis loop was measured in an applied magnetic field of ±20 kOe and the saturation magnetization was evaluated.

The compressive strength and modulus were evaluated using a universal testing machine (WD-D1, Shanghai Zhuoji Instrument Co., Ltd., Shanghai, China). The force-displacement curve was recorded automatically by a flat indenter with a slow loading speed of 0.5 mm/min. The compression strength and elastic modulus of the sample was calculated from the compression stress-strain curve. The hardness of composite scaffolds was assessed by a digital micro Vickers hardness tester (Micro Vickers Hardness Tester, HVS-1000C Shenzhen Shunhua Instrument Equipment Co., Ltd., Shenzhen, China) using an indentation test after polished. The Vickers hardness was calculated by the equation [33]: $HV = 0.1891F/d^2$, where F is the test force (N) and d is the diagonal length (mm). Each set of data was averaged and standard deviation from five replicate samples. The microscopic morphology of the surface pores and sections of the scaffold were characterized by scanning electron microscopy (SEM, Phenom ProX, Phenom-World BV, Eindhoven, Netherlands).

2.4. Cellular Compatibility

MG63 cells were cultured to evaluate the cell compatibility of scaffolds owning to their similar matrix synthesis and mineralization capabilities to osteoblasts. The cells were cultured in DMEM supplemented with sodium pyruvate, 10% FBS, 100 U/mL penicillin and 100 µg/mL streptomycin at 37 °C in a humidified 5% CO_2 atmosphere. The magnetic scaffold was sterilized with an ultraviolet lamp for 2 h and then placed in a 24 well culture plate for evaluation of cell adhesion and proliferation. MG63 cells were seeded at a density of 4×10^5 cells per well and the cultured medium was changed daily. After 1, 3, and 7 days of culture, the cell-scaffold samples were taken out, rinsed with PBS, immobilized using 4% glutaraldehyde for 30 min, dehydrated with ethanol for 24 h, and completely dried. After being sputtered with gold, the morphology of the cells on the scaffolds was observed by SEM. At each evaluation period, after the cells were stained with 2 µM calcein acetoxymethyl ester for 30 min, the fluorescence microscope equipped with a digital camera was used for observation and analysis.

The CCK-8 method was used to evaluate the proliferation of cells planted on the scaffolds. After 1.0×10^4 MG63 cells were planted on the scaffold and cultured for different days, 40 µl of CCK-8 solution was added to each well and incubated for 4 h, and the absorbance at 450 nm was measured by a microplate reader. The biological activity of the magnetic scaffolds was evaluated by evaluating the degree of differentiation of the cells by detecting the activity of alkaline phosphatase in the medium solution of the scaffold and osteoblasts. After the induction of MG63 cells for 3, 5, and 7 days, the scaffolds were taken out, washed with PBS. The cells were separated by 0.25% trypsin, transferred to a new 24 well plate medium, and washed three times with PBS. After fixing with formalin for 30 s and washing twice with deionized water, they were stained with ALP reagent for 1 h, and finally photographed by a microscope (TE2000U, Nikon Co., Tokyo, Japan).

2.5. Statistical Analysis

The quantitative data were expressed as mean ± standard error. The statistical difference was analyzed using student's t-test and $p < 0.05$ was considered as the level of significance, which is expressed as *.

3. Results and Discussion

3.1. Physicochemical Properties and Thermal Properties

The phase composition of the scaffold was analyzed using XRD (Figure 2a). PLLA shows two broad diffraction peaks at 16.5° and 19.9°, indicating that it was a semi-crystalline structure. Fe_3O_4 shows diffraction peaks at 30.1°, 35.4°, 43.1°, 53.5°, 57.0°, and 62.6°, which correspond to the crystal planes (220), (311), (400), (422), (511), and (440) [34]. These characteristic peaks of Fe_3O_4

were detected in the PLLA/Fe$_3$O$_4$ composite scaffold, and their intensity increased with the increase of its content, which confirmed that Fe$_3$O$_4$ was successfully introduced into the scaffold. Compared with the pure PLLA scaffold, the peak of PLLA in the composite scaffold was significantly weakened or even disappeared. This may be because the diffraction peak of Fe$_3$O$_4$ was too strong and the relative peak intensity of PLLA was weakened. In addition, the positions of the diffraction peaks of PLLA and Fe$_3$O$_4$ in the composite scaffold did not change, and no other peaks were observed, indicating that SLS preparation did not cause the formation of new phases or phase transformations.
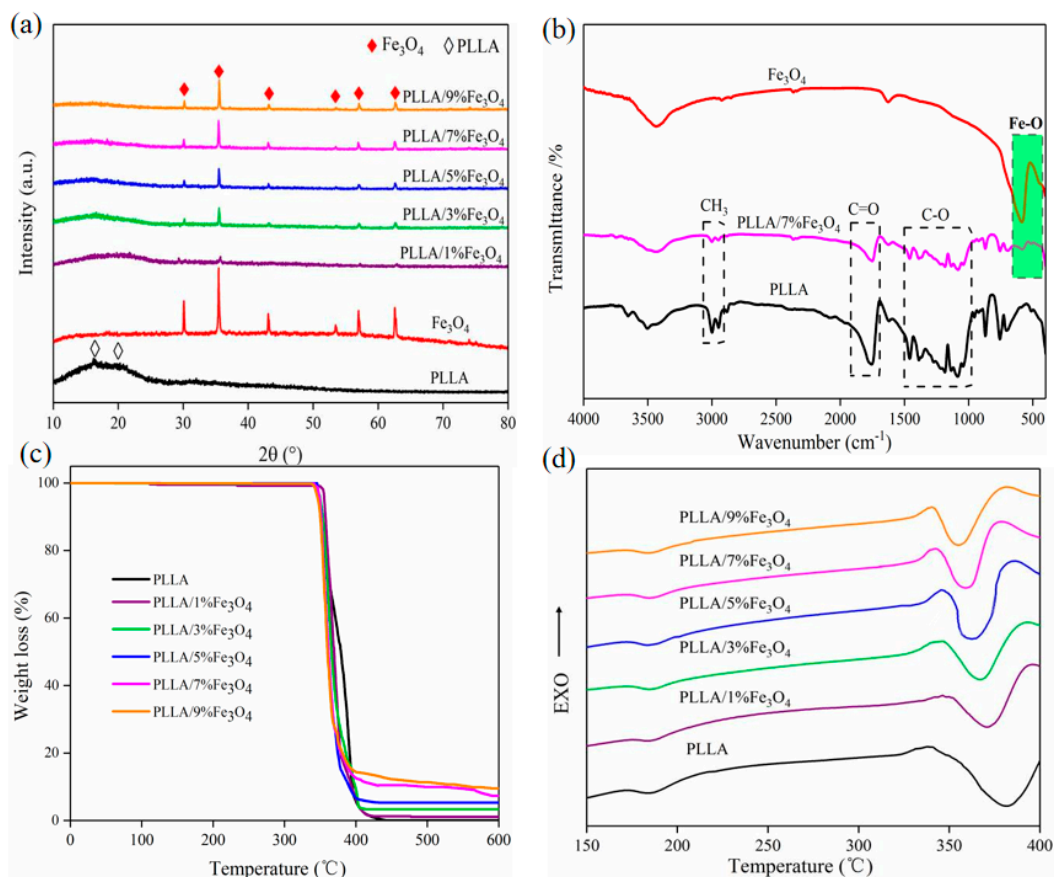

Figure 2. Physicochemical properties and thermal properties of the magnetic scaffolds with 0–9 wt % of Fe$_3$O$_4$ content. (**a**) XRD patterns. (**b**) FTIR patterns. (**c**) TGA profiles. (**d**) DSC profiles.

The chemical functional groups of the scaffold were analyzed using FTIR (Figure 2b). PLLA has characteristic absorption peaks at 3000, 1758, and 1500–1000 cm^{-1}, which correspond to the stretching vibration peaks of alkyl, carbonyl, and ether groups, respectively [35]. Fe$_3$O$_4$ has a characteristic absorption peak at 585 cm^{-1}, which corresponds to the stretching vibration peak of Fe-O [36]. This characteristic peak was also detected in the PLLA/7%Fe$_3$O$_4$ magnetic stent, which confirmed the successful introduction of Fe$_3$O$_4$ again. At the same time, several characteristic peaks of PLLA were clearly detected in the composite scaffold, which confirmed the existence of PLLA and made up for the results of XRD. The thermal stability of the composite scaffold was analyzed using DSC-TGA (Figure 2c,d). The magnetic scaffold exhibits significant thermal weight loss at 335~425 °C (Figure 2c), which was due to the thermal decomposition of PLLA [37]. After 425 °C, the residual weight of the scaffold hardly changed, which was due to the residual Fe$_3$O$_4$ with high thermal stability (melting point 1594.5 °C). The residual weight was about 0%, 1.2%, 3.4%, 5.2%, 7.6%, and 9.5%, respectively for PLLA/Fe$_3$O$_4$ scaffold with 0%, 1%, 3%, 5%, 7%, and 9% content, which was closed to the initial amount of Fe$_3$O$_4$ added. In the DSC curve, PLLA showed two endothermic peaks at 185.1 and 381.5 °C, which correspond to its melting temperature and decomposition temperature, respectively [30,38].

After Fe_3O_4 was added, the peak position at 185.1 °C did not change, indicating that the melting point of the scaffold did not change, but the position of the peak at 381.5 °C shifted slightly to the left, which means the thermal decomposition point decreased slightly. This may be due to the addition of Fe_3O_4 nanoparticles acting as a catalyst to accelerate the thermal decomposition of PLLA [39].

3.2. Magnetic Properties

The magnetic properties of the composite scaffolds at room temperature were qualitatively and quantitatively evaluated using permanent magnets and Vibrating Sample Magnetometer (Figure 3). As can be seen from the illustration in the upper left corner, the PLLA/7%Fe_3O_4 composite scaffold was firmly attracted by the permanent magnet from different sides, showing good magnetic properties. In the applied positive and negative magnetic fields (−20 kOe to +20 kOe), the magnetization curves of the scaffolds passed through the origin and were symmetrical at the origin without magnetization hysteresis, indicating that the scaffolds had good superparamagnetism [28]. The Ms is an extremely important parameter for magnetic performance evaluation, which refers to the maximum magnetization that can be achieved in a magnetic field [22,40]. The Ms of the composite scaffolds calculated from the magnetization curves are shown in the lower right corner of Figure 3. The value of Ms was positively related to the content of Fe_3O_4. In detail, the Ms of the 1%, 3%, 5%, 7%, and 9% Fe_3O_4 composite scaffolds were 1.1, 1.8, 2.5, 4.0, and 6.1 emu/g. These showed that the composite scaffold had strong magnetism.
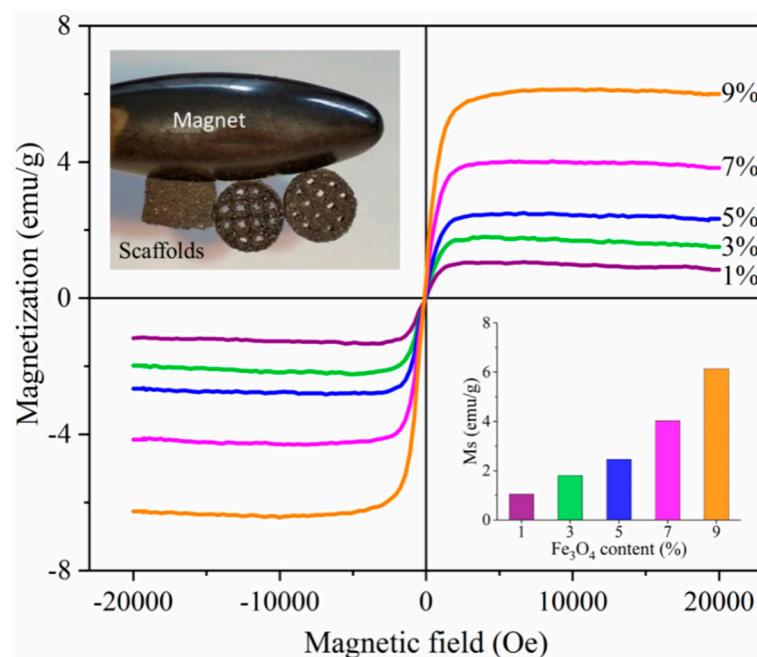

Figure 3. Magnetic properties of composite scaffolds. The main picture was the magnetization curves of the composite scaffolds in the magnetic field at room temperature. The illustration in the upper left corner was an optical view of the PLLA/7%Fe_3O_4 composite scaffold attracted by the permanent magnet from different sides. The illustration in the lower right corner was the saturation magnetization (Ms).

3.3. Mechanical Properties

Mechanical properties were of great importance for use as a bone scaffold because they provided mechanical support in bone repair. The stress-strain curves after the compression test of the scaffolds are shown in Figure 4a. The stress of all the scaffolds increases almost linearly with the strain at the initial stage, and then continues to increase to the maximum peak and then appears an inflection point. The peak was defined as the intensity, and the slope of the initial linear phase was defined as the strength. Then the compressive strength (Figure 4b) and compressive modulus (Figure 4c)

were calculated. The compressive strength and modulus in pure PLLA were 17.8 MPa and 1.6 GPa, respectively. After Fe_3O_4 was added, the compressive strength of the scaffold was improved. When the content of Fe_3O_4 was not more than 7%, the compressive strength increased with the content, and reached the maximum at 7%, which were 29.1 MPa and 2.9 GPa, increased by 63.4% and 78.9%, respectively. Then, when the Fe_3O_4 content was further increased to 9%, the compressive strength and modulus decreased compared to 7%, to 26.4 MPa and 2.7 GPa, but were still higher than pure PLLA. The change trend of the Vickers hardness of the scaffolds as a function of with the content of Fe_3O_4 was similar to the compression properties, and it reached the optimal value at 7%, which was 67.7 HV (Figure 4d).
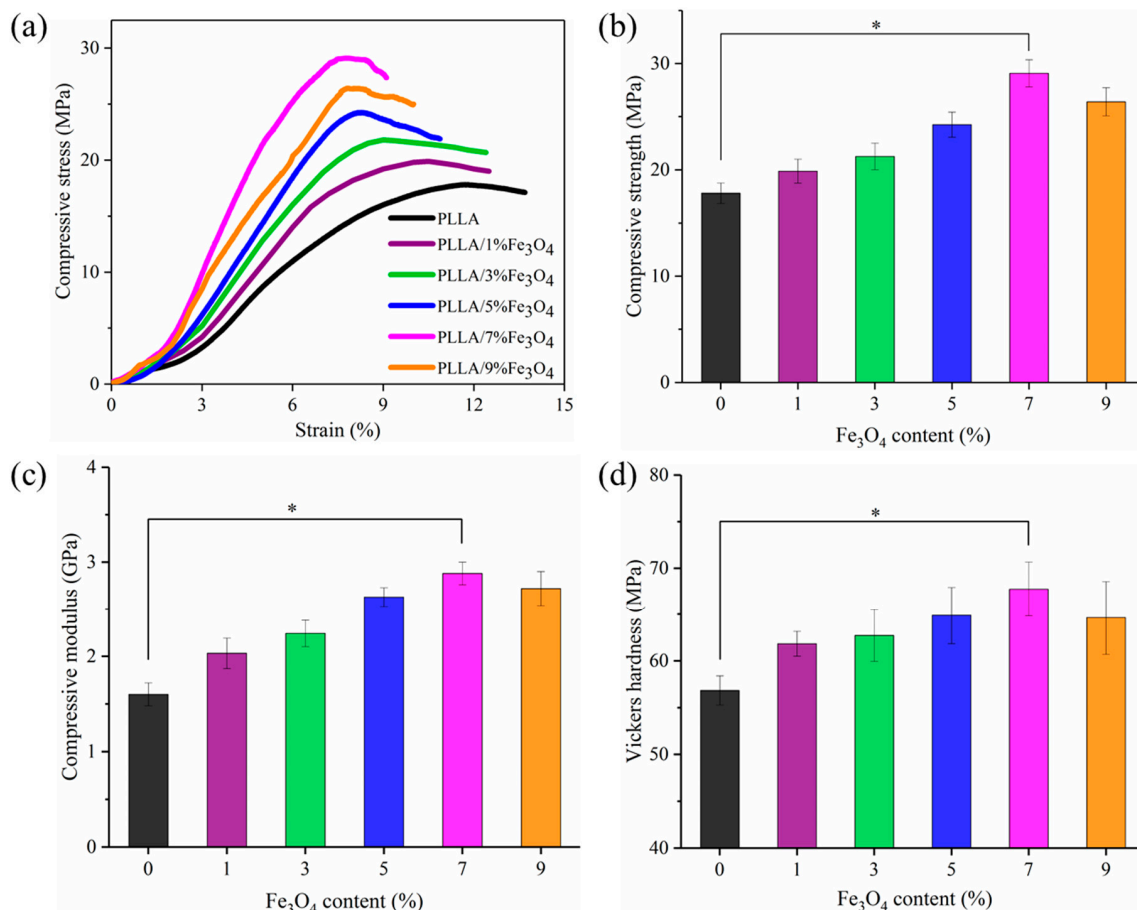
Figure 4. Mechanical properties of the scaffolds. (**a**) Stress-strain curve (**b**) Compressive strength (**c**) Compression modulus (**d**) Vickers hardness. * Represented significant difference ($p < 0.05$) when the PLLA/7%Fe_3O_4 scaffold compared with the pure PLLA scaffold.

The distribution of nano reinforcing phases was closely related to the mechanical properties of polymer nanocomposites. Therefore, the dispersion of Fe_3O_4 in the PLLA matrix was analyzed using SEM (Figure 5). The fracture surface of pure PLLA (Figure 5a) was relatively clean and smooth. After adding Fe_3O_4, the fracture surface became rough. Fe_3O_4 particles were randomly dispersed in the PLLA matrix. When the amount of Fe_3O_4 added was no more than 7% (Figure 5e), the number of Fe_3O_4 particles on the cross-section increased with the increase of the content of Fe_3O_4 added, and a good dispersion was maintained. However, when the Fe_3O_4 content was further increased to 9% (Figure 5f), obvious agglomeration began to appear in the scaffold.
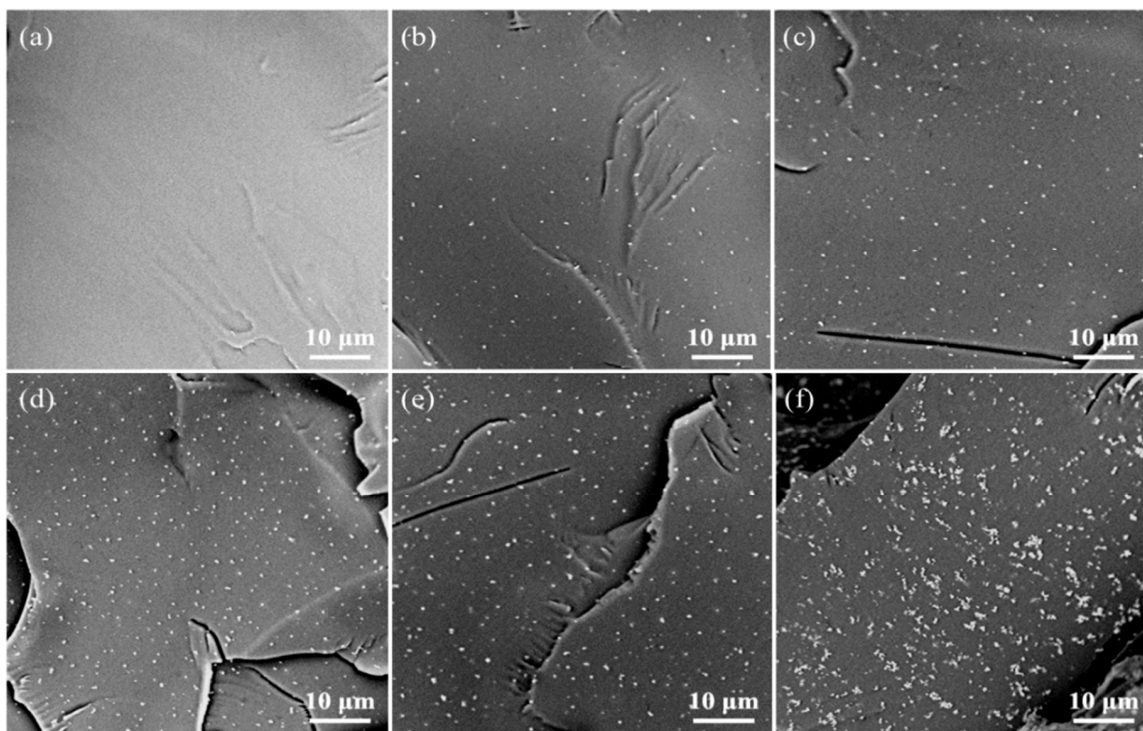
Figure 5. SEM images of fracture surfaces of scaffolds with different proportions. (**a**) PLLA scaffold, (**b**) PLLA/1%Fe$_3$O$_4$ scaffold, (**c**) PLLA/3%Fe$_3$O$_4$ scaffold, (**d**) PLLA/5%Fe$_3$O$_4$ scaffold, (**e**) PLLA/7%Fe$_3$O$_4$ scaffold, (**f**) PLLA/9%Fe$_3$O$_4$ scaffold.

Usually, on the premise of uniform dispersion, the more the amount of nanoparticles added, the better the enhancing effect [41]. When the Fe$_3$O$_4$ content was less than or equal to 7%, the uniformly dispersed Fe$_3$O$_4$ nanoparticles acted as a nanoscale reinforcement in the polymer matrix and reached a peak at 7%. However, when the content of Fe$_3$O$_4$ was continuously added to 9%, the excess Fe$_3$O$_4$ was difficult to uniformly disperse in the matrix, forming more agglomerates, which reduced the enhancement efficiency [42]. Therefore, the mechanical properties of the PLLA/9%Fe$_3$O$_4$ scaffold no longer continue to increase compared with 7% Fe$_3$O$_4$.

3.4. Cell Responses

Biocompatibility is very critical for the application of bone scaffolds [43,44]. Based on the previous experimental results, the PLLA/7%Fe$_3$O$_4$ scaffold with the best comprehensive performance was selected for further culture experiments. The adhesion and morphology of MG63 cells on the scaffolds were characterized by SEM observation (Figure 6). After MG63 cells were cultured on the scaffolds for 1 day, they were spindle-shaped or ellipsoidal. After three days of incubation, the cells expanded on the scaffolds, and obvious filamentous pseudopodia appeared, which helped the cells to adhere tightly to the scaffold and continue to grow. After seven days, the number of cells increased. The cells completely spread out on the surface of the scaffold, and there was a fusion between the cells. On the PLLA/7%Fe$_3$O$_4$ scaffold, it can be seen that they have been connected to form a fusion layer (Figure 6f). More importantly, MG63 cells exhibited better adhesion morphology and proliferation levels on PLLA/7%Fe$_3$O$_4$ scaffolds than pure PLLA scaffolds at the same culture time. These showed that the magnetic scaffold had good cell compatibility.
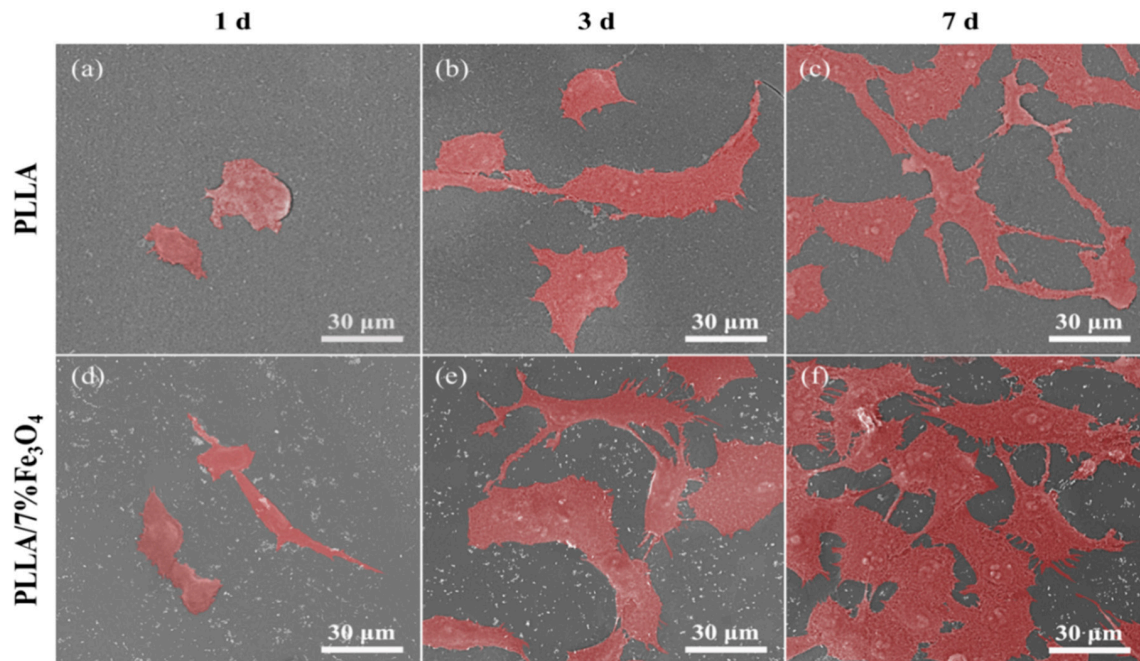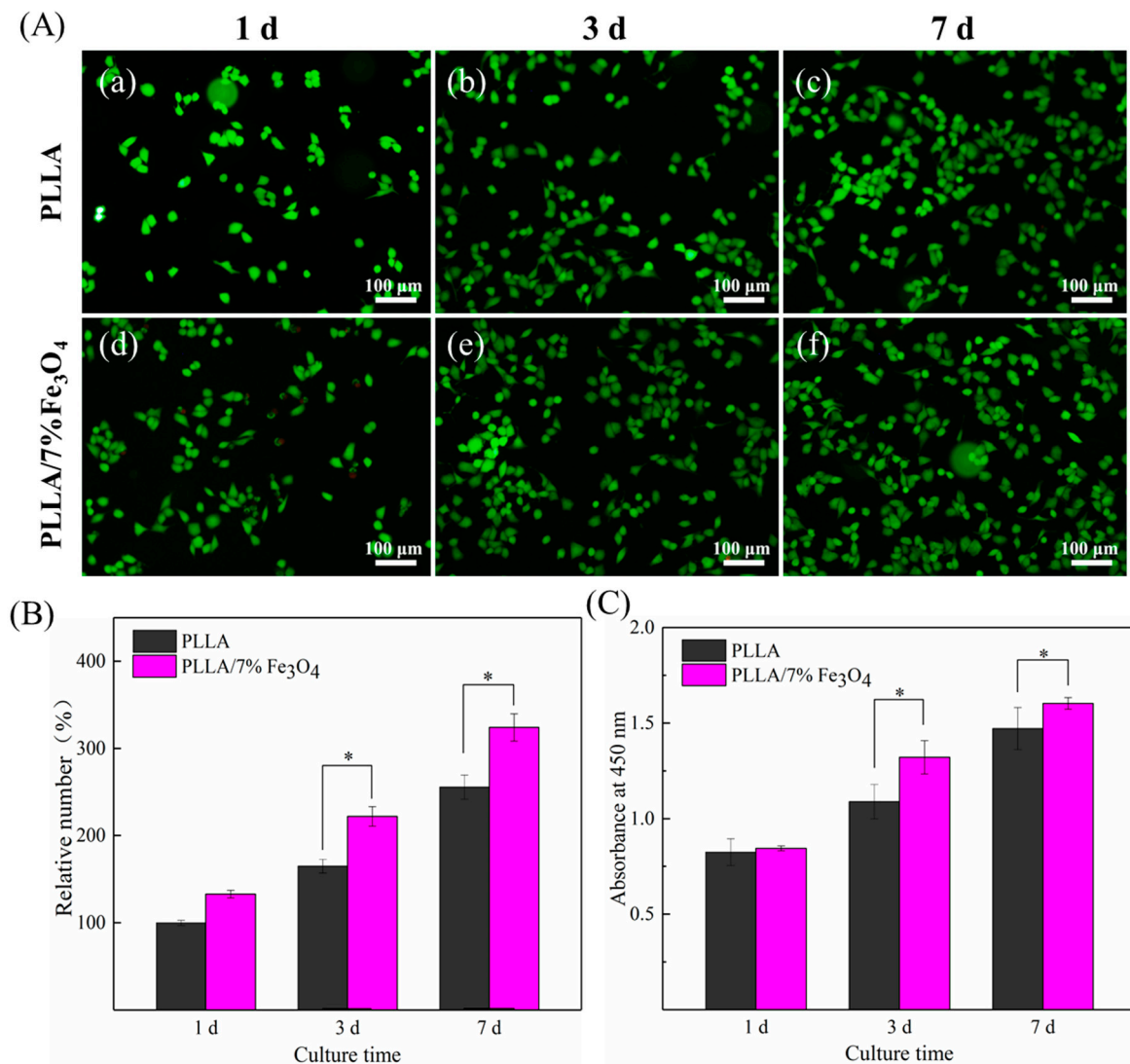
Figure 6. SEM pseudocolor image of MG63 cell adhesion on the scaffolds. (**a**) 1 day on the PLLA scaffold, (**b**) 3 days on the PLLA scaffold, (**c**) 7 days on the PLLA scaffold, (**d**) 1 day on the PLLA/7%Fe_3O_4 scaffold, (**e**) 3 days on the PLLA/7%Fe_3O_4 scaffold, (**f**) 7 days on the PLLA/7%Fe_3O_4 scaffold.

The behavior of MG63 cells on magnetic bone scaffolds was further studied using fluorescent staining. The results were shown in Figure 7. Obviously, compared with pure PLLA scaffold, there were more green fluorescent cells on magnetic bone scaffolds, and it was positively correlated with the culture time. Taking the number of cells on pure PLLA scaffolds after one day of culture as a 100% comparison, the statistical results are shown in Figure 7B. In order to further study the effect of magnetic scaffolds on the proliferation of MG63 cells, the CCK-8 test was used to evaluate the proliferation capacity of the scaffolds, and the results are shown in Figure 7C. After cell culture for three and seven days, the absorbance value (representing more living cells) on the PLLA/7%Fe_3O_4 scaffold was significantly higher than that of the pure PLLA scaffold ($p < 0.05$) indicating that the cell proliferation was enhanced [31]. It was shown that the Fe_3O_4 nanoparticles in the scaffolds could obviously promote the proliferation of MG63 cells.

ALP is a critical marker for the early differentiation of osteoblasts. Its activity was used to assess the level of differentiation of MG63 cells cultured on magnetic scaffolds (Figure 8). It can be seen from the stained image that the ALP activity increased with increasing culture time. The ALP activity on the magnetic scaffold was higher than the ALP activity on the pure PLLA scaffold, indicating that osteogenic differentiation of MG63 cells was significantly up-regulated, which indicated that the magnetic scaffold had the ability to stimulate MG63 cell differentiation ability.

It is well known that the components contained in the scaffold have a significant effect on the cellular response. Among them, Fe_3O_4 nanoparticles have strong magnetic features and unique superparamagnetic properties in nanometric dimensions. Meanwhile, the structure of cell membrane is complex. It not only contains charged lipid molecules, water, and protein, but also contains many ion channels such as K^+, Na^+, Ca^{2+} and so on. There is also a large amount of Cl^-, K^+, Na^+, and other anions and cations on the inner and outer surfaces of the membrane [45–47]. Therefore, Fe_3O_4 nanoparticles can serve as a magnetic source for a single magnetic nanofield in a weak electromagnetic field formed by the cell due to the difference between internal and external ions and charges, thereby generating a biological effect of magnetic field on cells [48–50]. Maleki-Ghaleh. H et al. reported that in this weak electromagnetic field of cells, Fe_3O_4 magnetic materials improved cell growth and activity by generating magnetic fields to enhance cell communication [24]. When it was combined with

the matrix, a large number of tiny magnetic fields were generated on the pores or the surface of the scaffold. According to previous studies, magnetic fields may affect the nucleation of protein crystals in the culture medium and the distribution of proteins in the cell membrane, accelerating the specific recognition of integrin proteins on the cell surface and adsorbing to the extracellular matrix proteins on the surface of the scaffold, thereby promoting cell adhesion and spread [29,51]. Meanwhile, magnetic field stimulation can activate calcium ion (Ca^{2+}) channels on the cell membrane, which can increase the concentration of calcium ions in cells, thereby improving the function of Ca^{2+}/calmodulin and the activity of cyclin-dependent kinase, promoting the proliferation of osteoblasts [52–54].

Figure 7. (**A**) Fluorescence image of MG63 cell culture on the scaffolds for 1, 3 and 7 days. (**a**) 1 day on the PLLA scaffold, (**b**) 3 days on the PLLA scaffold, (**c**) 7 days on the PLLA scaffold, (**d**) 1 day on the PLLA/7%Fe$_3$O$_4$ scaffold, (**e**) 3 days on the PLLA/7%Fe$_3$O$_4$ scaffold, (**f**) 7 days on the PLLA/7%Fe$_3$O$_4$ scaffold. (**B**) The relative number of living cells in the fluorescence graph. (**C**) CCK-8 graph.
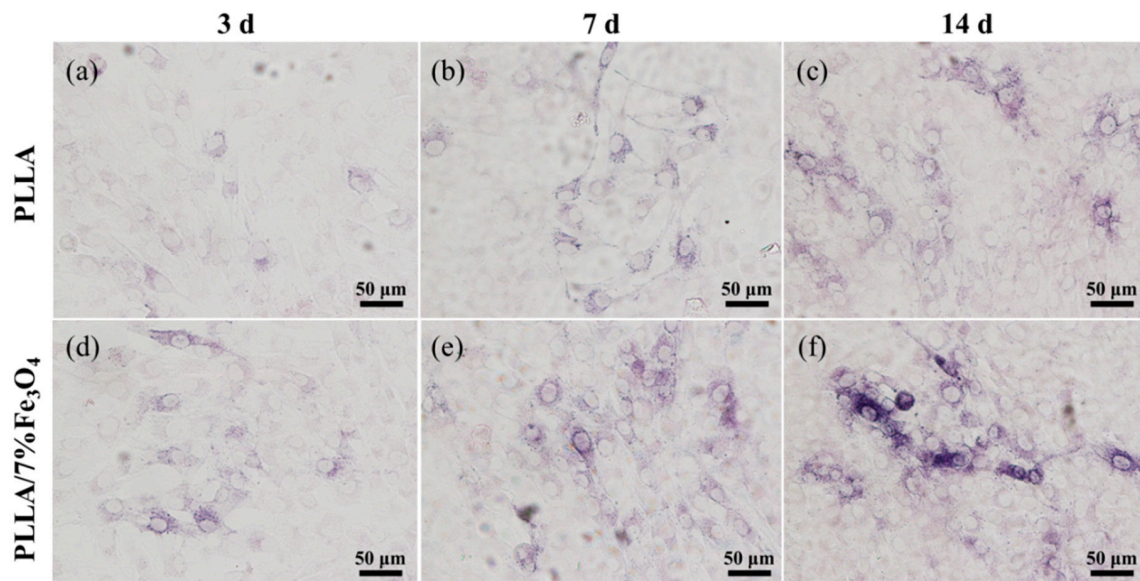
Figure 8. ALP activity staining diagram of MG63 cells on the scaffolds. (**a**) 3 days on the PLLA scaffold, (**b**) 7 days on the PLLA scaffold, (**c**) 14 days on the PLLA scaffold, (**d**) 3 days on the PLLA/7% Fe_3O_4 scaffold, (**e**) 7 days on the PLLA/7%Fe_3O_4 scaffold, (**f**) 14 days on the PLLA/7% Fe_3O_4 scaffold.

In addition, the magnetic field can also activate various signal pathways of the cell, and collaboratively mediate the signal communication between them, such as the classic mitogen-activated protein kinase [55–57] and BMP signal pathway [17,58], thereby promoting the expression of growth factors, improving the activity of runt-related transcription factor 2 and ALP, accelerating the growth and differentiation of osteoblasts, and promoting bone repair finally. Of course, the micro magnetic force generated in the microenvironment of the magnetic scaffold can provide continuous dynamic mechanical stimulation to MG63 cells, which can also improve the cells adhere and migrate. In addition, the Fe_3O_4 nanoparticles in the scaffold have a large surface area to volume ratio. Uniform dispersion in the scaffold may show more contact surface area, thus providing more attachment sites for cell attachment [59]. However, the Fe_3O_4 nanoparticles are nanomaterials, and previous studies have indicated that the nanomaterials may cause some potential adverse effects on cells and organs of the human body [60–62]. For example, Long et al. [60] investigated the effect of Fe_3O_4 nanoparticles on cell activity of human hepatoma cell and lung adenocarcinoma cell, and their results indicated that the higher concentration of Fe_3O_4 nanoparticles would cause cell death. PLLA is a biodegradable and biocompatibility bone scaffold material which has a relatively low degradation rate [63,64]. When the Fe_3O_4 nanoparticles are incorporated into the PLLA scaffold, the slow degradation of scaffold can play the role of controlled release of Fe_3O_4 nanoparticles, thereby continuously and steadily enhancing cellular activity without causing adverse effects to human body.

4. Conclusions

In this study, PLLA/Fe_3O_4 scaffolds were successfully fabricated by SLS. The incorporated Fe_3O_4 nanoparticles not only enhance the mechanical properties of the PLLA scaffold, but also effectively improve the biological activity of the scaffold. The results showed that the PLLA/7%Fe_3O_4 composite scaffold exhibited increased compressive strength, modulus, and Vickers hardness, which were 29.1 MPa, 2.9 GPa, and 67.7 HV, respectively. Furthermore, the magnetic composite scaffold not only promoted cell attachment, diffusion, and interaction, but also significantly promoted MG63 cell proliferation and stimulated cell differentiation. All these positive results suggested that the SLS-processed PLLA/Fe_3O_4 scaffold was of great potential for bone regeneration.

Author Contributions: Conceptualization, S.B. and A.W.; Methodology, S.B.; Validation, P.F.; Formal Analysis, W.G.; Investigation, S.B.; Resources, P.F.; Data Curation, W.G.; Writing—Original Draft Preparation, S.B.;

References

1. Islami, M.; Mortazavi, Y.; Soleimani, M.; Nadri, S. In vitro expansion of CD 133+ cells derived from umbilical cord blood in poly-L-lactic acid (PLLA) scaffold coated with fibronectin and collagen. *Artif. Cells Nanomed. Biotechnol.* **2018**, *46*, 1025–1033. [CrossRef]

2. Yusof, M.R.; Shamsudin, R.; Zakaria, S.; Abdul Hamid, M.A.; Yalcinkaya, F.; Abdullah, Y.; Yacob, N. Fabrication and characterization of carboxymethyl starch/poly (l-lactide) acid/β-tricalcium phosphate composite nanofibers via electrospinning. *Polymers* **2019**, *11*, 1468. [CrossRef]

3. Shamsah, A.H.; Cartmell, S.H.; Richardson, S.M.; Bosworth, L.A. Material Characterization of PCL: PLLA Electrospun Fibers Following Six Months Degradation In Vitro. *Polymers* **2020**, *12*, 700. [CrossRef]

4. Shuai, C.; Liu, G.; Yang, Y.; Qi, F.; Peng, S.; Yang, W.; He, C.; Wang, G.; Qian, G. A strawberry-like Ag-decorated barium titanate enhances piezoelectric and antibacterial activities of polymer scaffold. *Nano Energy* **2020**, *74*, 104825. [CrossRef]

5. Shuai, C.; Yu, L.; Feng, P.; Zhong, Y.; Zhao, Z.; Chen, Z.; Yang, W. Organic montmorillonite produced an interlayer locking effect in a polymer scaffold to enhance interfacial bonding. *Mater. Chem. Front.* **2020**, *4*, 2398–2408. [CrossRef]

6. Birhanu, G.; Akbari Javar, H.; Seyedjafari, E.; Zandi-Karimi, A.; Dusti Telgerd, M. An improved surface for enhanced stem cell proliferation and osteogenic differentiation using electrospun composite PLLA/P123 scaffold. *Artif. Cells Nanomed. Biotechnol.* **2018**, *46*, 1274–1281. [CrossRef] [PubMed]

7. Castillejos, S.; Cerna, J.; Meléndez, F.; Castro, M.E.; Aguilar, R.; Márquez-Beltrán, C.; González, M. Bulk Modification of Poly (lactide)(PLA) via Copolymerization with Poly (propylene glycol) Diglycidylether (PPGDGE). *Polymers* **2018**, *10*, 1184. [CrossRef] [PubMed]

8. Schofer, M.D.; Roessler, P.P.; Schaefer, J.; Theisen, C.; Schlimme, S.; Heverhagen, J.T.; Voelker, M.; Dersch, R.; Agarwal, S.; Fuchs-Winkelmann, S. Electrospun PLLA nanofiber scaffolds and their use in combination with BMP-2 for reconstruction of bone defects. *PLoS ONE* **2011**, *6*, e25462. [CrossRef]

9. Zhu, W.; Chen, K.; Lu, W.; Sun, Q.; Peng, L.; Fen, W.; Li, H.; Ou, Y.; Liu, H.; Wang, D. In vitro study of nano-HA/PLLA composite scaffold for rabbit BMSC differentiation under TGF-β1 induction. *In Vitro Cell. Dev. Biol. Anim.* **2014**, *50*, 214–220. [CrossRef]

10. Çakır-Özkan, N.; Eğri, S.; Bekar, E.; Altunkaynak, B.Z.; Kabak, Y.B.; Kıvrak, E.G. The use of sequential VEGF-and BMP2-releasing biodegradable scaffolds in rabbit mandibular defects. *J. Oral Maxillofac. Surg.* **2017**, *75*, 221.e1–221.e14.

11. Murahashi, Y.; Yano, F.; Nakamoto, H.; Maenohara, Y.; Iba, K.; Yamashita, T.; Tanaka, S.; Ishihara, K.; Okamura, Y.; Moro, T. Multi-layered PLLA-nanosheets loaded with FGF-2 induce robust bone regeneration with controlled release in critical-sized mouse femoral defects. *Acta Biomater.* **2019**, *85*, 172–179. [CrossRef]

12. Hesari, R.; Keshvarinia, M.; Kabiri, M.; Rad, I.; Parivar, K.; Hoseinpoor, H.; Tavakoli, R.; Soleimani, M.; Kouhkan, F.; Zamanluee, S. Comparative impact of platelet rich plasma and transforming growth factor-β on chondrogenic differentiation of human adipose derived stem cells. *Bioimpacts* **2020**, *10*, 37. [CrossRef]

13. Huang, K.-C.; Yano, F.; Murahashi, Y.; Takano, S.; Kitaura, Y.; Chang, S.H.; Soma, K.; Ueng, S.W.; Tanaka, S.; Ishihara, K. Sandwich-type PLLA-nanosheets loaded with BMP-2 induce bone regeneration in critical-sized mouse calvarial defects. *Acta Biomater.* **2017**, *59*, 12–20. [CrossRef] [PubMed]

14. Mohammadi, M.; Alibolandi, M.; Abnous, K.; Salmasi, Z.; Jaafari, M.R.; Ramezani, M. Fabrication of hybrid scaffold based on hydroxyapatite-biodegradable nanofibers incorporated with liposomal formulation of BMP-2 peptide for bone tissue engineering. *Nanomed. Nanotechnol. Biol. Med.* **2018**, *14*, 1987–1997. [CrossRef] [PubMed]

15. Zhang, J.; Meng, X.; Ding, C.; Shang, P. Effects of static magnetic fields on bone microstructure and mechanical properties in mice. *Electromagn. Biol. Med.* **2018**, *37*, 76–83. [CrossRef] [PubMed]

16. Zhu, Y.; Yang, Q.; Yang, M.; Zhan, X.; Lan, F.; He, J.; Gu, Z.; Wu, Y. Protein corona of magnetic hydroxyapatite scaffold improves cell proliferation via activation of mitogen-activated protein kinase signaling pathway. *ACS Nano* **2017**, *11*, 3690–3704. [CrossRef]

17. Yuan, Z.; Memarzadeh, K.; Stephen, A.S.; Allaker, R.P.; Brown, R.A.; Huang, J. Development of a 3D collagen model for the in vitro evaluation of magnetic-assisted osteogenesis. *Sci. Rep.* **2018**, *8*, 1–11. [CrossRef]

18. Yin, G.; Huang, Z.; Deng, M.; Zeng, J.; Gu, J. Preparation and cell response of bio-mineralized Fe_3O_4 nanoparticles. *J. Colloid Interface Sci.* **2011**, *363*, 393–402. [CrossRef]

19. Yew, Y.P.; Shameli, K.; Miyake, M.; Khairudin, N.B.B.A.; Mohamad, S.E.B.; Naiki, T.; Lee, K.X. Green biosynthesis of superparamagnetic magnetite Fe_3O_4 nanoparticles and biomedical applications in targeted anticancer drug delivery system: A review. *Arab. J. Chem.* **2020**, *13*, 2287–2308. [CrossRef]

20. Ghazanfari, M.R.; Kashefi, M.; Shams, S.F.; Jaafari, M.R. Perspective of Fe_3O_4 nanoparticles role in biomedical applications. *Biochem. Res. Int.* **2016**. [CrossRef]

21. Nehra, P.; Chauhan, R.; Garg, N.; Verma, K. Antibacterial and antifungal activity of chitosan coated iron oxide nanoparticles. *Br. J. Biomed. Sci.* **2018**, *75*, 13–18. [CrossRef]

22. Zhang, L.; Zhang, Y. Fabrication and magnetic properties of Fe_3O_4 nanowire arrays in different diameters. *J. Magn. Magn. Mater.* **2009**, *321*, L15–L20. [CrossRef]

23. Sodipo, B.K.; Aziz, A.A. Recent advances in synthesis and surface modification of superparamagnetic iron oxide nanoparticles with silica. *J. Magn. Magn. Mater.* **2016**, *416*, 275–291. [CrossRef]

24. Maleki-Ghaleh, H.; Aghaie, E.; Nadernezhad, A.; Zargarzadeh, M.; Khakzad, A.; Shakeri, M.; Khosrowshahi, Y.B.; Siadati, M. Influence of Fe 3 O 4 nanoparticles in hydroxyapatite scaffolds on proliferation of primary human fibroblast cells. *J. Mater. Eng. Perform.* **2016**, *25*, 2331–2339. [CrossRef]

25. Bourrinet, P.; Bengele, H.H.; Bonnemain, B.; Dencausse, A.; Idee, J.-M.; Jacobs, P.M.; Lewis, J.M. Preclinical safety and pharmacokinetic profile of ferumoxtran-10, an ultrasmall superparamagnetic iron oxide magnetic resonance contrast agent. *Investig. Radiol.* **2006**, *41*, 313–324. [CrossRef]

26. Chen, L.; Peng, J.; Zhao, J.; Long, Y.; Xie, Y.; Nie, J. Magnetic Materials in Promoting Bone Regeneration. *Front. Mater.* **2019**, *6*, 268.

27. Cunha, C.; Panseri, S.; Iannazzo, D.; Piperno, A.; Pistone, A.; Fazio, M.; Russo, A.; Marcacci, M.; Galvagno, S. Hybrid composites made of multiwalled carbon nanotubes functionalized with Fe_3O_4 nanoparticles for tissue engineering applications. *Nanotechnology* **2012**, *23*, 465102. [CrossRef]

28. Shan, D.; Shi, Y.; Duan, S.; Wei, Y.; Cai, Q.; Yang, X. Electrospun magnetic poly (L-lactide)(PLLA) nanofibers by incorporating PLLA-stabilized Fe_3O_4 nanoparticles. *Mater. Sci. Eng. C* **2013**, *33*, 3498–3505. [CrossRef]

29. Wu, Y.; Jiang, W.; Wen, X.; He, B.; Zeng, X.; Wang, G.; Gu, Z. A novel calcium phosphate ceramic–magnetic nanoparticle composite as a potential bone substitute. *Biomed. Mater.* **2010**, *5*, 015001. [CrossRef]

30. Wei, Y.; Zhang, X.; Song, Y.; Han, B.; Hu, X.; Wang, X.; Lin, Y.; Deng, X. Magnetic biodegradable Fe_3O_4/CS/PVA nanofibrous membranes for bone regeneration. *Biomed. Mater.* **2011**, *6*, 055008. [CrossRef]

31. Cai, Q.; Shi, Y.; Shan, D.; Jia, W.; Duan, S.; Deng, X.; Yang, X. Osteogenic differentiation of MC3T3-E1 cells on poly (l-lactide)/Fe_3O_4 nanofibers with static magnetic field exposure. *Mater. Sci. Eng. C* **2015**, *55*, 166–173. [CrossRef]

32. Qin, T.; Li, X.; Long, H.; Bin, S.; Xu, Y. Bioactive Tetracalcium Phosphate Scaffolds Fabricated by Selective Laser Sintering for Bone Regeneration Applications. *Materials* **2020**, *13*, 2268. [CrossRef]

33. Moqbel, N.M.; Al-Akhali, M.; Wille, S.; Kern, M. Influence of Aging on Biaxial Flexural Strength and Hardness of Translucent 3Y-TZP. *Materials* **2020**, *13*, 27. [CrossRef]

34. Shahabadi, N.; Falsafi, M.; Mansouri, K. Improving antiproliferative effect of the anticancer drug cytarabine on human promyelocytic leukemia cells by coating on Fe_3O_4@SiO_2 nanoparticles. *Colloids Surf. B Biointerfaces* **2016**, *141*, 213–222. [CrossRef]

35. Li, J.; Li, Y.; Li, L.; Mak, A.F.; Ko, F.; Qin, L. Preparation and biodegradation of electrospun PLLA/keratin nonwoven fibrous membrane. *Polym. Degrad. Stab.* **2009**, *94*, 1800–1807. [CrossRef]

36. Zhang, D.; Karki, A.B.; Rutman, D.; Young, D.P.; Wang, A.; Cocke, D.; Ho, T.H.; Guo, Z. Electrospun polyacrylonitrile nanocomposite fibers reinforced with Fe_3O_4 nanoparticles: Fabrication and property analysis. *Polymer* **2009**, *50*, 4189–4198. [CrossRef]

37. Yin, G.; Zhao, D.; Ren, Y.; Zhang, L.; Zhou, Z.; Li, Q. A convenient process to fabricate gelatin modified porous PLLA materials with high hydrophilicity and strength. *Biomater. Sci.* **2016**, *4*, 310–318. [CrossRef]

38. Shuai, C.; Li, Y.; Wang, G.; Yang, W.; Peng, S.; Feng, P. Surface modification of nanodiamond: Toward the dispersion of reinforced phase in poly-l-lactic acid scaffolds. *Int. J. Biol. Macromol.* **2019**, *126*, 1116–1124. [CrossRef]

39. Yang, W.; Zhong, Y.; Feng, P.; Gao, C.; Peng, S.; Zhao, Z.; Shuai, C. Disperse magnetic sources constructed with functionalized Fe_3O_4 nanoparticles in poly-l-lactic acid scaffolds. *Polym. Test.* **2019**, *76*, 33–42. [CrossRef]

40. Irez, A.; Bayraktar, E.; Miskioglu, I. Recycled and devulcanized rubber modified epoxy-based composites reinforced with nano-magnetic iron oxide, Fe_3O_4. *Compos. Part. B Eng.* **2018**, *148*, 1–13. [CrossRef]

41. Shuai, C.; Wang, B.; Bin, S.; Peng, S.; Gao, C. TiO_2 induced in situ reaction in graphene oxide reinforced AZ61 biocomposites to enhance the interfacial bonding. *ACS Appl. Mater. Interfaces* **2020**, *12*, 23464–23473. [CrossRef] [PubMed]

42. Shuai, C.; Yu, L.; Feng, P.; Gao, C.; Peng, S. Interfacial reinforcement in bioceramic/biopolymer composite bone scaffold: The role of coupling agent. *Colloids Surf. B Biointerfaces* **2020**, *193*, 111083. [CrossRef] [PubMed]

43. Dong, Z.; Li, Y.; Zou, Q. Degradation and biocompatibility of porous nano-hydroxyapatite/polyurethane composite scaffold for bone tissue engineering. *Appl. Surf. Sci.* **2009**, *255*, 6087–6091. [CrossRef]

44. Saber-Samandari, S.; Mohammadi-Aghdam, M.; Saber-Samandari, S. A novel magnetic bifunctional nanocomposite scaffold for photothermal therapy and tissue engineering. *Int. J. Biol. Macromol.* **2019**, *138*, 810–818. [CrossRef]

45. Blank, M. Protein and DNA reactions stimulated by electromagnetic fields. *Electr. Magn. Biol. Med.* **2008**, *27*, 3. [CrossRef] [PubMed]

46. Cifra, M.; Fields, J.Z.; Farhadi, A. Electromagnetic cellular interactions. *Prog. Biophys. Mol. Biol.* **2011**, *105*, 223–246. [CrossRef] [PubMed]

47. Ikehara, T.; Yamaguchi, H.; Miyamoto, H. Effect of electromagnetic fields on membrane ion transport of cultured cells. *J. Med. Investig.* **1998**, *45*, 47–56.

48. Yan, X.; Song, G.; Wang, X.; Zhao, Y.; Chen, Y. The preparation and medical applications of chitosan microspheres. *Curr. Org. Chem.* **2018**, *22*, 720–733. [CrossRef]

49. Adey, W.R. Biological effects of electromagnetic fields. *J. Cell. Biochem.* **1993**, *51*, 410–416. [CrossRef]

50. Gorgun, S.S. Studies on the interaction between electromagnetic fields and living matter neoplastic cellular culture. *Cent. Front. Sci. Thmple Univ.* **1998**, *7*, 1–21.

51. Huang, D.-M.; Hsiao, J.-K.; Chen, Y.-C.; Chien, L.-Y.; Yao, M.; Chen, Y.-K.; Ko, B.-S.; Hsu, S.-C.; Tai, L.-A.; Cheng, H.-Y. The promotion of human mesenchymal stem cell proliferation by superparamagnetic iron oxide nanoparticles. *Biomaterials* **2009**, *30*, 3645–3651. [CrossRef] [PubMed]

52. Rubio, M.A.; Syrovets, T.; Hafner, S.; Zablotskii, V.; Dejneka, A.; Simmet, T. Spatiotemporal magnetic fields enhance cytosolic Ca2+ levels and induce actin polymerization via activation of voltage-gated sodium channels in skeletal muscle cells. *Biomaterials* **2018**, *163*, 174–184. [CrossRef] [PubMed]

53. Tay, A.; Kunze, A.; Murray, C.; Di Carlo, D. Induction of calcium influx in cortical neural networks by nanomagnetic forces. *Acs Nano* **2016**, *10*, 2331–2341. [CrossRef]

54. Yap, J.L.Y.; Tai, Y.K.; Fröhlich, J.; Fong, C.H.H.; Yin, J.N.; Foo, Z.L.; Ramanan, S.; Beyer, C.; Toh, S.J.; Casarosa, M. Ambient and supplemental magnetic fields promote myogenesis via a TRPC1—mitochondrial axis: Evidence of a magnetic mitohormetic mechanism. *FASEB J.* **2019**, *33*, 12853–12872. [CrossRef]

55. Wu, X.; Du, J.; Song, W.; Cao, M.; Chen, S.; Xia, R. Weak power frequency magnetic fields induce microtubule cytoskeleton reorganization depending on the epidermal growth factor receptor and the calcium related signaling. *PLoS ONE* **2018**, *13*, e0205569. [CrossRef]

56. Lew, W.Z.; Feng, S.W.; Lin, C.T.; Huang, H.M. Use of 0.4—Tesla static magnetic field to promote reparative dentine formation of dental pulp stem cells through activation of p38 MAPK signalling pathway. *Int. Endod. J.* **2019**, *52*, 28–43. [CrossRef]

57. Yun, H.-M.; Kang, S.-K.; Singh, R.K.; Lee, J.-H.; Lee, H.-H.; Park, K.-R.; Yi, J.-K.; Lee, D.-W.; Kim, H.-W.; Kim, E.-C. Magnetic nanofiber scaffold-induced stimulation of odontogenesis and pro-angiogenesis of human dental pulp cells through Wnt/MAPK/NF-κB pathways. *Dent. Mater.* **2016**, *32*, 1301–1311. [CrossRef]

58. Li, W.; Zhao, S.; He, W.; Zhang, M.; Li, S.; Xu, Y. Static magnetic fields accelerate osteogenesis by regulating FLRT/BMP pathway. *Biochem. Biophys. Res. Commun.* **2020**, *527*, 83–89. [CrossRef]

59. Yang, W.; Zhong, Y.; He, C.; Peng, S.; Yang, Y.; Qi, F.; Feng, P.; Shuai, C. Electrostatic self-assembly of pFe_3O_4 nanoparticles on graphene oxide: A co-dispersed nanosystem reinforces PLLA scaffolds. *J. Adv. Res.* **2020**, *24*, 191–203. [CrossRef]

60. Long, L.; Yuan, Z.; Yin, L.P.; Liu, R.; Huang, B.L.; Liu, S.Y. An observation on effect of pure magnetic nanoparticles (Fe_3O_4) on human hepatoma cells and human lung adenocarcinoma cells. *J. Toxicol.* **2009**, *23*, 89–92.

61. Huang, X.; Ma, P.; Rao, Y.; Zhao, W.; Yang, X. Pulmonary biosafety of Fe_3O_4 nanoparticles used in sports engineering on Kunming mice. *Ferroelectrics* **2018**, *527*, 44–51. [CrossRef]

62. Park, E.J.; Umh, H.N.; Choi, D.H.; Cho, M.H.; Choi, W.; Kim, S.W.; Kim, Y.; Kim, J.H. Magnetite- and maghemite-induced different toxicity in murine alveolar macrophage cells. *Arch. Toxicol.* **2014**, *88*, 1607–1618. [CrossRef]

63. Wojasiński, M.; Faliszewski, K.; Ciach, T. Electrospinning production of PLLA fibrous scaffolds for tissue engineering. *Chall. Mod. Technol.* **2013**, *4*, 9–15.

64. Chen, H.M.; Feng, C.X.; Zhang, W.B.; Yang, J.H.; Huang, T.; Zhang, N.; Wang, Y. Hydrolytic degradation behavior of poly (l-lactide)/carbon nanotubes nanocomposites. *Polym. Degrad. Stab.* **2013**, *98*, 198–208. [CrossRef]